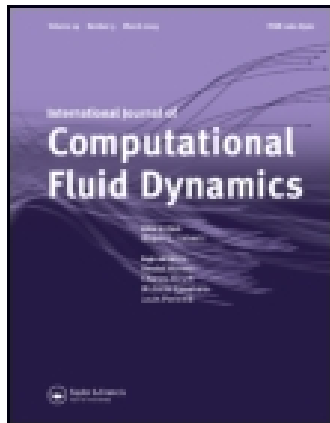


This article was downloaded by: [Huazhong University of Science & Technology]

On: 26 December 2014, At: 20:25

Publisher: Taylor & Francis

Informa Ltd Registered in England and Wales Registered Number: 1072954 Registered office: Mortimer House, 37-41 Mortimer Street, London W1T 3JH, UK



International Journal of Computational Fluid Dynamics

Publication details, including instructions for authors and subscription information:

<http://www.tandfonline.com/loi/gcfd20>

An integrated 2-D Navier-Stokes equation and its application to 3-D internal flows

A. Nakayama^a, F. Kuwahara^a & W. Liu^b

^a Shizuoka University, Department of Mechanical Engineering, 3-5-1 Johoku, Hamamatsu, 432-8561, Japan

^b School of Energy and Power Engineering, Huazhong University of Science and Technology, Wuhan, 430074, P.R. China

Published online: 25 Jan 2007.

To cite this article: A. Nakayama, F. Kuwahara & W. Liu (2006) An integrated 2-D Navier-Stokes equation and its application to 3-D internal flows, International Journal of Computational Fluid Dynamics, 20:2, 99-104, DOI: [10.1080/10618560600595371](https://doi.org/10.1080/10618560600595371)

To link to this article: <http://dx.doi.org/10.1080/10618560600595371>

PLEASE SCROLL DOWN FOR ARTICLE

Taylor & Francis makes every effort to ensure the accuracy of all the information (the "Content") contained in the publications on our platform. However, Taylor & Francis, our agents, and our licensors make no representations or warranties whatsoever as to the accuracy, completeness, or suitability for any purpose of the Content. Any opinions and views expressed in this publication are the opinions and views of the authors, and are not the views of or endorsed by Taylor & Francis. The accuracy of the Content should not be relied upon and should be independently verified with primary sources of information. Taylor and Francis shall not be liable for any losses, actions, claims, proceedings, demands, costs, expenses, damages, and other liabilities whatsoever or howsoever caused arising directly or indirectly in connection with, in relation to or arising out of the use of the Content.

This article may be used for research, teaching, and private study purposes. Any substantial or systematic reproduction, redistribution, reselling, loan, sub-licensing, systematic supply, or distribution in any form to anyone is expressly forbidden. Terms & Conditions of access and use can be found at <http://www.tandfonline.com/page/terms-and-conditions>

An integrated 2-D Navier–Stokes equation and its application to 3-D internal flows

A. NAKAYAMA†*, F. KUWAHARA† and W. LIU‡

†Department of Mechanical Engineering, Shizuoka University, 3-5-1 Johoku, Hamamatsu 432-8561, Japan

‡School of Energy and Power Engineering, Huazhong University of Science and Technology, Wuhan 430074, P.R. China

An efficient two-dimensional (2-D) analytical and numerical procedure has been proposed to investigate three-dimensional (3-D) internal flows through a passage with a spatially variable depth, in which the viscous forces act significantly on both upper and lower walls. The integral 2-D version of the Navier–Stokes equation was obtained by integrating the full Navier–Stokes equation in a 3-D form over the depth of the passage. In order to examine the validity of the integrated momentum equations, fully-developed flows in straight noncircular ducts were investigated analytically prior to numerical investigations. It has been shown that the exact solutions for circular, elliptical and equilateral triangular ducts are obtainable from the integrated Navier–Stokes equation. Having confirmed its wide applicability to internal flows, numerical computations were conducted to investigate the oscillation mechanism of a fluidic oscillator. Comparison of the present prediction and experiment reveals the validity of the present treatment.

Keywords: Internal flow; Numerical method; Fluidics; Oscillation; Non-circular ducts

Nomenclature

f	velocity profile function
$h(x, y)$	half depth of the passage, function for the wall geometry,
u, v, w	velocity components in the x, y and z directions
\bar{u}, \bar{v}	average velocity components
u_{in}	bulk mean velocity at the nozzle inlet
p	pressure
$Re_{L_{in}} = \frac{u_{in} L_{in}}{\nu}$	Reynolds number based on L_{in} and u_{in}
$St = \frac{f L_{in}}{u_{in}}$	Strouhal number
t	time
x, y, z	Cartesian coordinates
ν	kinematic viscosity
ρ	density
$\zeta = \frac{z}{h(x,y)}$	dimensionless coordinate
Subscript	
in	nozzle inlet

1. Introduction

Internal flows encountered in engineering applications are three-dimensional (3-D) in nature. Hence, we often have

to appeal to 3-D computations in order to capture the details of velocity and pressure fields for designing heat and fluid flow equipment. Such 3-D computations, however, are extremely expensive and time consuming, even when only steady state solutions are required. Ironically, we may find it difficult to extract meaningful flow characteristics directly from the results obtained in such 3-D computations, because of excess spatial information. Thus, having completed full 3-D computations, the 3-D results are often integrated over a certain coordinate to reduce to the averaged values. Such averaged quantities are much easier to appreciate, making it possible for us to draw the overall aspects of 3-D flow characteristics much better.

Recent advances in microfabrication technologies have been so promising that some micro-fluidics may compete with conventional mechanical and electrical systems. Fluidic devices such as feedback fluidic oscillators (e.g. Trippetts *et al.* 1973, Parry *et al.* 1991, Zemel and Furlan 1996) and fluidic flowmeters (e.g. Boucher and Mazharoglu 1988, Mansy and Williams 1989, Lua and Zheng 2003) consist of complex 3-D passages with a small depth.

The foregoing consideration prompts us to introduce an efficient two-dimensional (2-D) numerical calculation procedure for a 3-D internal flow through a passage with a spatially variable depth, in which the viscous forces act

*Corresponding author. Email: tmanaka@ipc.shizuoka.ac.jp

significantly on both upper and lower walls. We shall derive such a set of 2-D governing equations by integrating the full 3-D Navier–Stokes equation over the depth. The resulting integrated momentum equations will be solved for the dependent variables, namely, the mean velocity components and pressure averaged locally over the depth, which varies spatially.

An analytically reduced version of the integrated momentum equation is applied for the problems of fully-developed flows in noncircular ducts, so as to restore a class of exact solutions, which are known for noncircular shapes. In this way, the soundness of the integrated momentum equation is elucidated. Furthermore, this set of the integrated momentum equations is discretized using a finite volume method, so as to conform with SIMPLE algorithm. A numerical experiment is conducted to investigate the oscillation mechanism of a feedback fluidic oscillator, which is designed to spray water to an automobile windshield. The frequency predicted by the present numerical procedure is in good accord with that of the experiment, which proves the validity of the present economical numerical procedure.

2. Two-dimensional Navier–Stokes equation integrated over the depth

We shall consider complex passages such as used in fluidic oscillators for spraying water to the automobile windshield, as shown in figure 1. We assume that the passage is shallow enough for the flow within the passage to stay laminar. The governing equations in consideration, namely, the continuity, Navier–Stokes and energy equations for incompressible flows are given by

$$\frac{\partial u}{\partial x} + \frac{\partial v}{\partial y} + \frac{\partial w}{\partial z} = 0 \quad (1)$$

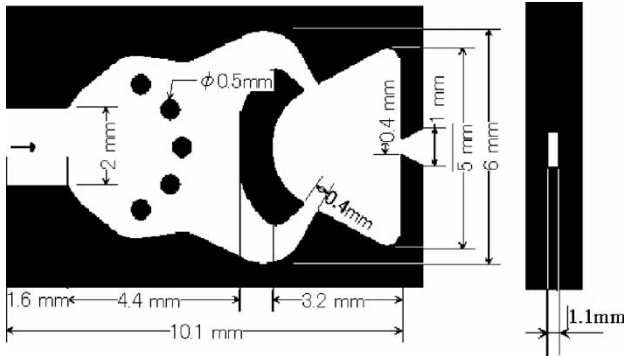


Figure 1. Fluidic oscillator used for spraying water.

$$\begin{aligned} & \frac{\partial u}{\partial t} + \frac{\partial}{\partial x} \left(u^2 - \nu \frac{\partial u}{\partial x} \right) + \frac{\partial}{\partial y} \left(vu - \nu \frac{\partial u}{\partial y} \right) \\ & + \frac{\partial}{\partial z} \left(wu - \nu \frac{\partial u}{\partial z} \right) \\ & = -\frac{1}{\rho} \frac{\partial p}{\partial x} \end{aligned} \quad (2)$$

$$\begin{aligned} & \frac{\partial v}{\partial t} + \frac{\partial}{\partial x} \left(uv - \nu \frac{\partial v}{\partial x} \right) + \frac{\partial}{\partial y} \left(v^2 - \nu \frac{\partial v}{\partial y} \right) \\ & + \frac{\partial}{\partial z} \left(wv - \nu \frac{\partial v}{\partial z} \right) \\ & = -\frac{1}{\rho} \frac{\partial p}{\partial y} \end{aligned} \quad (3)$$

$$\begin{aligned} & \frac{\partial w}{\partial t} + \frac{\partial}{\partial x} \left(uw - \nu \frac{\partial w}{\partial x} \right) + \frac{\partial}{\partial y} \left(vw - \nu \frac{\partial w}{\partial y} \right) \\ & + \frac{\partial}{\partial z} \left(w^2 - \nu \frac{\partial w}{\partial z} \right) \\ & = -\frac{1}{\rho} \frac{\partial p}{\partial z}. \end{aligned} \quad (4)$$

The passage in consideration is symmetric with respect to the x - y plane such that the upper and lower wall geometries are given by $z = \pm h(x, y)$, respectively. The following procedure appears to be similar to that of Hele–Shaw flow. However, it is noted that $h(x, y)$ can vary spatially, and that both inertial and viscous terms are retained. We integrate the continuity equation from 0 to $h(x, y)$ with respect to z as:

$$\frac{\partial}{\partial x} \int_0^h u \, dz + \frac{\partial}{\partial y} \int_0^h v \, dz = 0. \quad (5)$$

We assume the velocity profiles are:

$$\begin{aligned} u(t, x, y, z) &= \bar{u}(t, x, y) f(\zeta) \quad \text{and} \\ v(t, x, y, z) &= \bar{v}(t, x, y) f(\zeta) \end{aligned} \quad (6)$$

where

$$\zeta = \frac{z}{h(x, y)} \quad (7)$$

and $\bar{u}(x, y)$ and $\bar{v}(x, y)$ are the velocity components averaged over the depth, such that the symmetric function $f(\zeta)$ should satisfy

$$f(\pm 1) = 0 \quad \text{and} \quad f'(0) = 0. \quad (8)$$

The foregoing integral form of the continuity equation (5) may be rewritten as

$$\frac{\partial \bar{u}h}{\partial x} + \frac{\partial \bar{v}h}{\partial y} = 0. \quad (9)$$

Since $w(x, y, z) \approx 0$, the z -momentum equation (4) immediately gives $p = p(t, x, y)$. We substitute the velocity profiles given by equation (6) and $p = p(t, x, y)$ into the x - and y -momentum equations (2) and (3), and then integrate them over the depth to find

$$\begin{aligned} h \frac{\partial \bar{u}}{\partial t} + \frac{\partial}{\partial x} \left(h \bar{u}^2 - \nu \frac{\partial h \bar{u}}{\partial x} \right) + \frac{\partial}{\partial y} \left(h \bar{v} \bar{u} - \nu \frac{\partial h \bar{u}}{\partial y} \right) \\ = -\frac{h \partial p}{\rho \partial x} + \nu f'(1) \frac{\bar{u}}{h} \left(1 + \left(\frac{\partial h}{\partial x} \right)^2 + \left(\frac{\partial h}{\partial y} \right)^2 \right) \end{aligned} \quad (10)$$

$$\begin{aligned} h \frac{\partial \bar{v}}{\partial t} + \frac{\partial}{\partial x} \left(h \bar{u} \bar{v} - \nu \frac{\partial h \bar{v}}{\partial x} \right) + \frac{\partial}{\partial y} \left(h \bar{v}^2 - \nu \frac{\partial h \bar{v}}{\partial y} \right) \\ = -\frac{h \partial p}{\rho \partial y} + \nu f'(1) \frac{\bar{v}}{h} \left(1 + \left(\frac{\partial h}{\partial x} \right)^2 + \left(\frac{\partial h}{\partial y} \right)^2 \right). \end{aligned} \quad (11)$$

One of the simplest candidates for the symmetric function $f(\zeta)$ is assumed as:

$$f(\zeta) = \frac{3}{2}(1 - \zeta^2) \quad (12)$$

such that $f'(1) = -3$. The profile given by the function conforms to the no-slip and symmetry conditions given by equation (8). The integrated momentum equations (10) and (11) along with the integrated continuity equation (9) form a complete set of the governing equations for a 3-D internal flow through a complex passage with a small depth. These governing equations subject to no-slip conditions are believed to be valid for all passages described by a moderately varying arbitrary function $h(x, y)$.

3. Fully developed flows in noncircular ducts

We shall examine the validity of the integrated momentum equations, considering fully developed flows in straight noncircular ducts, as shown in figure 2.

For the case of fully developed flows, the integrated set of the equations reduce to the following ordinary differential equation in a dimensionless form as:

$$\frac{d^2}{dy^{*2}} h^* \bar{u}^* - 3 \frac{\bar{u}^*}{h^*} \left(1 + \left(\frac{dh^*}{dy^*} \right)^2 \right) + h^* = 0 \quad (13)$$

where

$$\bar{u}^* \equiv \frac{\bar{u}}{\left(-\frac{L_{\text{ref}}^2}{\mu} \frac{dp}{dx} \right)}, \quad h^* \equiv \frac{h}{L_{\text{ref}}} \quad \text{and} \quad y^* \equiv \frac{y}{L_{\text{ref}}}. \quad (14)$$

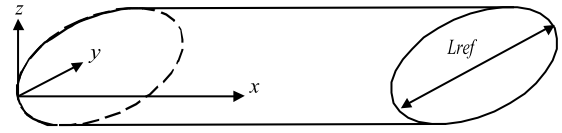


Figure 2. Coordinate system for a straight noncircular duct.

The duct width may be chosen for the reference length L_{ref} , as shown in figure 3. As the duct shape $h^*(y^*; 0 \leq y^* \leq 1)$ is given, the foregoing second order O.D.E. may be solved for $\bar{u}^*(y^*)$ using the obvious boundary conditions, namely,

$$\bar{u}^*(0) = \bar{u}^*(1) = 0. \quad (15)$$

Instead of specifying a particular duct shape, $h^*(y^*)$, to find its vertically averaged velocity profile $\bar{u}^*(y^*)$, we shall take an inverse solution procedure. That is to find a family of possible duct shape functions $h^*(y^*)$, upon assuming the velocity profile function in the form of

$$\bar{u}^*(y^*) = cy^* a(1 - y^*)^b \quad (16)$$

such that it automatically satisfies the boundary conditions given by equation (15). Substitution of the foregoing velocity function (16) into equation (13) and some manipulation lead to

$$\begin{aligned} \bar{u}^*(y^*) = cy^* a(1 - y^*)^b \\ = -\left(\frac{1}{h^*} \frac{d^2 h^*}{dy^{*2}} + 2 \left(\frac{a}{y^*} - \frac{b}{1 - y^*} \right) \frac{1}{h^*} \frac{dh^*}{dy^*} \right. \\ \left. + \left(\frac{a(a-1)}{y^{*2}} - \frac{2ab}{y^*(1-y^*)} + \frac{b(b-1)}{(1-y^*)^2} \right) \right. \\ \left. - \frac{3}{h^* 2} \left(1 + \left(\frac{dh^*}{dy^*} \right)^2 \right) \right)^{-1}. \end{aligned} \quad (17)$$

We note the constancy of the exponents a and b in the foregoing expression, and find the family of possible duct shape functions, namely, $h^* = (1/\sqrt{3})y^*$ and $h^* = \gamma\sqrt{y^*(1-y^*)}$, which correspond to the cases of

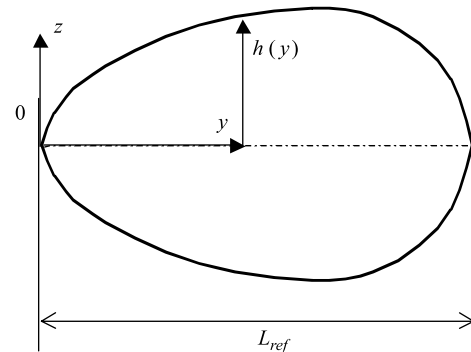


Figure 3. Cross-sectional view of noncircular duct.

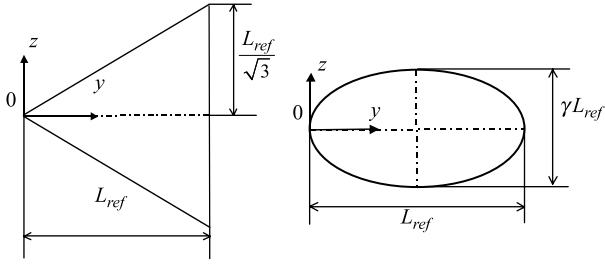


Figure 4. Duct cross-sections: (a) Equilateral triangular cross-section; (b) Elliptical cross-section.

equilateral triangle and elliptical sections, respectively, as shown in figure 4(a) and (b).

Equilateral triangle of side $2L_{\text{ref}}/\sqrt{3}$:

$$\bar{u}^* = \frac{1}{6}y^{*2}(1 - y^*) \quad \text{for} \quad h^* = \frac{1}{\sqrt{3}}y^* \quad (18)$$

and elliptical section with axes L_{ref} and γL_{ref} :

$$\begin{aligned} \bar{u}^* &= \frac{\gamma^2}{3(1 + \gamma^2)}y^{*2}(1 - y^*) \quad \text{for} \\ h^* &= \gamma\sqrt{y^*(1 - y^*)}. \end{aligned} \quad (19)$$

These dimensionless functions for the average velocity can be translated to find the local velocity field over the duct cross-section

$$u(y, z) = \left(-\frac{L_{\text{ref}}^2}{\mu} \frac{dp}{dx}\right) \bar{u}^* \left(\frac{y}{L_{\text{ref}}}\right) f\left(\frac{z}{h}\right)$$

as equilateral triangle of side $2L_{\text{ref}}/\sqrt{3}$:

$$\begin{aligned} u(y, z) &= \frac{1}{4} \left(-\frac{L_{\text{ref}}^2}{\mu} \frac{dp}{dx}\right) \left(1 - \frac{y}{L_{\text{ref}}}\right) \\ &\quad \times \left(\left(\frac{y}{L_{\text{ref}}}\right)^2 - 3\left(\frac{z}{L_{\text{ref}}}\right)^2\right) \end{aligned} \quad (20)$$

and elliptical section with axes L_{ref} and γL_{ref} :

$$\begin{aligned} u(y, z) &= \frac{\gamma^2}{2(1 + \gamma^2)} \left(-\frac{L_{\text{ref}}}{\mu} \frac{dp}{dx}\right) \\ &\quad \times \left(\frac{y}{L_{\text{ref}}}\left(1 - \frac{y}{L_{\text{ref}}}\right) - \left(\frac{z}{L_{\text{ref}}}\right)^2\right) \end{aligned} \quad (21)$$

which turn out to be the exact solutions obtainable directly from Navier–Stokes equation (e.g. White 1974). Equation (21) for the case of $\gamma = 1$ reduces to the well-known

profile of Hagen–Poiseuille flow, namely,

$$u(r) = \frac{1}{4} \left(-\frac{1}{\mu} \frac{dp}{dx}\right) (R^2 - r^2) \quad (22)$$

where

$$R = L_{\text{ref}}/2 \quad \text{and} \quad r^2 = (y - R)^2 + z^2. \quad (23)$$

The foregoing preliminary consideration suggests a wide range of applicability of the present integral momentum equations.

4. Numerical simulation of jets from a fluidic oscillator

In what follows, the fluidic oscillator with constant h , as already shown in figure 1, will be examined numerically, using the integrated momentum equations (10) and (11) along with the integrated continuity equation (9). This oscillator is one of typical fluidic devices installed in some Japanese automobiles for spraying water to the automobile windshield. The numerical results obtained here are compared with the experimental data recently conducted by Kuwahara *et al.* (2005) so as to investigate the validity of this economical numerical procedure and its acquired accuracy.

All governing equations conform to the following general transport equation:

$$\begin{aligned} h \frac{\partial \phi}{\partial t} + \frac{\partial}{\partial x} \left(h \bar{u} \phi - \Gamma_\phi \frac{\partial h \phi}{\partial x} \right) \\ + \frac{\partial}{\partial y} \left(h \bar{v} \phi - \Gamma_\phi \frac{\partial h \phi}{\partial y} \right) = S_\phi \end{aligned} \quad (24)$$

which was then integrated over a small element and time interval to form a general discretized equation for the point P and its neighboring points E , W , N and S , as follows:

$$a_P \phi_P = a_E \phi_E + a_W \phi_W + a_N \phi_N + a_S \phi_S + b. \quad (25)$$

The well-known QUICK scheme has been adopted for differencing the advection terms. Then, they were numerically solved using SIMPLE algorithm proposed by Patankar and Spalding (1972). Convergence was measured in terms of the maximum change in each variable during an iteration. The maximum change allowed for the convergence check was set to 10^{-5} , as the variables are normalized by appropriate references. Further details on this numerical procedure can be found in Patankar (1980) and Nakayama (1995). All computations were performed using the computer system at Shizuoka University Computer Center.

In this study, the Cartesian grid system is used instead of the body fitted system. The latter is recommended if the detailed flow field within the passage needs to be explored. However, when only macroscopic characteristics such as

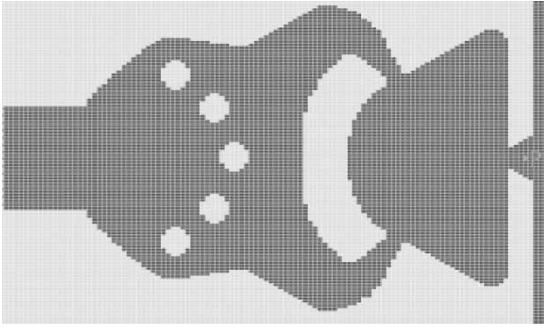


Figure 5. Grid nodes within the fluidic oscillator.

oscillation frequency are needed, the former would suffice for the purpose. Geometrical data from a CAD are first translated in a set of bmp data, which is then fed into the pre-processor developed by our group to generate a grid system automatically.

A typical grid system consists of 201×201 nodes with dense and coarse meshes for the regions inside and outside of the passages, respectively, to cover a large domain of integration, including both the fluidic device and its surroundings, namely, $100 \times 25 \text{ mm}^2$. Figure 5 shows a part of dense mesh distributed around the fluidic oscillator for the present non-uniform grid system. Preliminary calculations were made to compare the results against those obtained with 301×301 nodes for some selected

cases. In this way, the originally used grid resolution was found sufficient. Moreover, the time step was set small enough to satisfy Courant condition, after confirming that any further decrease in the time step does not alter the results significantly.

Numerical computations were initiated setting a uniform velocity u_{in} at the nozzle inlet, which was varied from 2.2 to 6.0 m/s, at the inlet. For this operation range, the Reynolds number $Re_{L_{\text{in}}}$ based on the inlet width L_{in} and velocity u_{in} varies from 4400 to 12,000. This is the range in which Kuwahara *et al.* (2005) previously conducted an experiment to measure the frequency of oscillating flow by a stroboscope. It takes about 10 cycles of oscillations for the velocity to attain its periodically fully-developed stage. Figure 6 (a)–(f) depict a complete cycle of the periodically fully-developed velocity field for the case of $Re_{L_{\text{in}}} = 4400$. These figures clearly show that the oscillation frequency for this case is about $f = 1/2.22 \text{ ms} = 450 \text{ Hz}$. The results of computations carried out for the fluidic oscillator were assembled in terms of Strouhal number $St \equiv fL_{\text{in}}/u_{\text{in}}$. The predicted Strouhal number St stays almost constant, namely, $St \equiv fL_{\text{in}}/u_{\text{in}} \approx 0.4$, over the range of Reynolds number studied, which turns out to be quite close to the experimentally observed value.

The mechanism of the fluidic oscillation is quite complex, as can be seen from these figures. Another set

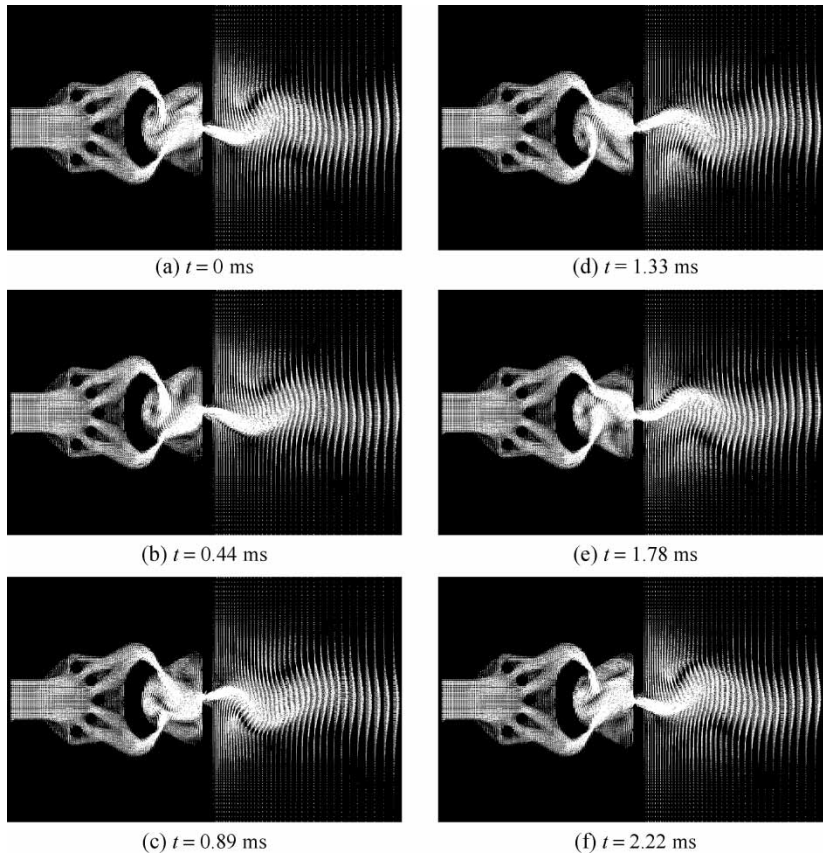


Figure 6. Oscillating velocity field.

of computations were carried out deleting five circular cylinder obstacles located upstream of the round equilateral triangular cavity. Oscillations were observed just as in the case of the passage with the obstacles. Thus, it is not the upstream flow obstruction but the imbalance in two jets meeting each other within the round equilateral triangular cavity that causes such fluidic oscillations. A parametric study can readily be made to find possible geometrical parameters to control its oscillation pattern and frequency, since the interface between the present CFD code and CAD system has been already established. However, such an attempt is out of the scope of the present study.

5. Concluding remarks

Full Navier–Stokes equation in the 3-D form was integrated over a local channel depth to obtain the integrated 2-D Navier–Stokes equation for analyzing 3-D internal flows through a passage with a spatially variable depth. Firstly, the integrated momentum equation was applied for the problems of laminar fully-developed flows in noncircular ducts, so as to restore a class of exact solutions, namely those for circular, elliptical and equilateral ducts. Secondly, a numerical computation code was developed and coupled with a CAD system, so as to conduct a numerical experiment, demonstrating its effectiveness for designing fluid flow devices. The numerical procedure developed in this study can easily be extended to the case of turbulent flows. Some friction law should be introduced to evaluate the turbulent frictional forces on the upper and lower walls. Such investigations are underway.

Acknowledgements

The authors would like to express their sincere thanks to President Morikawa, Technical Division Head Kageyama and Senior Researcher Tsukamoto of Nihon Biniron Co., Hamamatsu, Japan, for their support.

References

- Boucher, R.F. and Mazharoglu, C., Low Reynolds number fluidic flowmetering. *J. Phys. E: Sci. Instrum.*, 1988, **21**, 977–989.
- Kuwahara, F., Okazaki, S. and Nakayama, A., A three-dimensional internal flow through a complex passage with a small depth. *42nd National Heat Transfer Symposium of Japan*, 2005, **III**, 699–700.
- Lua, A.C. and Zheng, Z., Numerical simulations and experimental studies on a target fluidic flow meter. *Flow Meas. Instrum.*, 2003, **14**, 43–49.
- Mansy, H. and Williams, D.R., An experimental and numerical study of trapped vortex pair fluidic flowmeter. *ASME FED Forum on Turbulent Flows*, 1989, **76**, 35–39.
- Nakayama, A., *PC-Aided Numerical Heat Transfer and Convective Flow*, 1995 (CRC Press: Boca Raton).
- Parry, A.J., Chiwanga, S.G., Kalsi, H.S. and Jepson, P., Numerical and experimental visualization of flow through a target fluidic oscillator. *ASME FED Experimental and Numerical Flow Visualization*, 1991, **128**, 327–334.
- Patankar, S.V. and Spalding, D.B., A calculation procedure for heat, mass and momentum transfer in three-dimensional parabolic flows. *Int. J. Heat Mass Transfer*, 1972, **15**, 1787–1806.
- Patankar, S.V., *Numerical Heat Transfer and Fluid Flow*, 1980 (Hemisphere: Washington, DC).
- Trippetts, J.R., Ng, H.K. and Royle, J.K., An oscillating bistable fluid amplifier for use as a flowmeter. *Fluidics Q.*, 1973, **5**(1).
- White, F.M., *Viscous Fluid Flow*, pp. 123–124, 1974 (McGraw-Hill Book Company: New York).
- Zemel, J.N. and Furlan, R., *Microfluidics, Handbook of Chemical and Biological Sensors*, edited by R.F. Taylor and J.S. Schultz, pp. 317–347, 1996 (Institute of Physics Publishing: Bristol and Philadelphia).